Hindawi
Journal of Chemistry
Volume 2022, Article ID 4056110, 8 pages
https://doi.org/10.1155/2022/4056110

Research Article

Synthesis, Structure, and Hydrolytic Activation of Ruthenium (III)-Pyrazole Complex

Mylene Planques,[1] Arushi Shyam,[2] Richard S. Perkins,[2] Frank R. Fronczek,[3] and Radhey S. Srivastava[2]

[1]*Department of Chemistry, University of Poitiers, Poitiers, France*
[2]*Department of Chemistry, University of Louisiana, Lafayette, LA 70504, USA*
[3]*Department of Chemistry, Louisiana State University, Baton Rouge, LA 70803, USA*

Correspondence should be addressed to Radhey S. Srivastava; rss1805@louisiana.edu

Received 9 August 2022; Revised 9 September 2022; Accepted 5 October 2022; Published 17 December 2022

Academic Editor: Liviu Mitu

We report here the synthesis of water-soluble *mer*-[$RuCl_3$(DMSO-S) $(pyz)_2$] **2** prepared by the reaction of *mer*-$RuCl_3$(DMSO-S)$_3$ **1** with pyrazole in anhydrous CH_2Cl_2. Compound **2** was characterized by IR and UV-visible spectroscopy, X-ray diffraction, cyclic voltammetry, and DFT calculations. The X-ray diffraction analysis disclosed that compound **2** has two independent molecules present in the asymmetric unit with different conformations for one of the pyrazoles and different hydrogen bonding. The DFT calculations suggest the structure-activity relationship and hydrolytic activity of these complexes.

1. Introduction

The platinum-derived drugs are used in over half of all chemotherapy treatments [1–3] with severe side effects (intrinsic and acquired) [4–6]. This stimulated us to search for a new generation of cytotoxic drugs with other metals that may surpass cellular selectivity and maintain their usage against a broad range of malignancies [7–11]. The interest in Ru(III) complexes has increased considerably after the success of several platinum drugs [12]. Among all ruthenium anticancer compounds, ruthenium-DMSO complexes assumed a great potential for their selectivity and low host toxicity [13]. Accordingly, various ruthenium complexes have been found to exhibit a substantially higher extent of selectivity towards malignant cells compared to the prominent commercially available platinum drugs while resulting in reduced damage to healthy tissues [14].

A broadly believed mechanistic hypothesis of the selective delivery of Ru(III) complexes to cancer is the ability of ruthenium (III) complexes to mimic iron in reversible binding to plasma proteins such as transferrin. This hypothesis offers an efficient channel for ruthenium complexes to accumulate in cancer cells [15, 16]. Despite extensive efforts, only three ruthenium complexes, two structurally related Ru(III) compounds, NAMI-A ((ImH)[*trans*-$RuCl_4$(DMSO-S) (Im)], Im = imidazole) [17, 18], KP1019/KP1339 (KP1019 = (IndH)[*trans*-$RuCl_4(Ind)_2$], Ind = indazole; KP1339 = Na[*trans*-$RuCl_4(Ind)_2$]) have reached to the clinical evaluation stage in humans, opening the way to large expectations for a new class of metal-based anticancer drugs.

Ruthenium complexes, NAMI-A and KP1019/1339, are derivatives of imidazole/indazole (heterocyclic amines). Pyrazoles have electron-rich properties that can be altered by proper selection of substituents in various places in the pyrazole ring (e.g., 2N, 3C, 4C, and 5C), allowing electronic property optimization on the metal. Despite this, Ru-pyrazole complexes are poorly developed. Moreover, the complex **2** reported herein is water-soluble, which makes it attractive for being developed as a drug. Thus, we report herein the synthesis, structure, hydrolytic activity, and theoretical studies of the complex 2.

2. Experimental

2.1. General Information. Analytical grade reagents were used. The solvents were dried over 4 Å molecular sieves. The IR and UV-vis spectra were measured on a JASCO 480 spectrophotometer. Elemental analysis was performed by Atlantic Microlab in Norcross, Georgia, and $[H(DMSO)_2]$ [*trans*-$RuCl_4(DMSO)_2$] and *mer*-$[RuCl_3(DMSO\text{-}S)_2(DMSO\text{-}O)]$ complexes were prepared according to the literature procedures [19].

X-ray diffraction data were collected at low temperature on a Nonius Kappa CCD diffractometer equipped with Mo Kα radiation source ($\lambda = 0.71073$ Å), a graphite monochromator, and an Oxford cryostream low-temperature device. Absorption collections were made by the multiscan method. Data collection parameters and selected bond angles and lengths are listed in Tables 1 and 2.

2.2. Synthesis of mer-[$RuCl_3$(DMSO) (pyrazole)$_2$] 2. A solution of *mer*-$RuCl_3(DMSO)_3$ (0.27 g, 0.61 mmol) **1** and pyrazole (0.048 g, 0.63 mmol) in anhydrous CH_2Cl_2 were mixed and stirred at room temperature for about 20 h to get an orange solution. The orange solution, which was evaporated to 3 mL. A few drops of hexane were added, and the solution was kept in the refrigerator at −20°C. After a few hours, red crystals were formed, filtered off, washed with diethyl ether, and vacuum dried. Yield 0.248 g (0.49 mmol, 80%); Anal. Calcd. for $C_8H_{14}C_{l3}N_4ORuS$ (Mr = 424.71, %): C, 22.78; H, 3.35, N, 13.29; Found: C, 22.93; H, 3.24; N, 13.25; Selected IR absorption bands in KBr (cm^{-1}): ν_{SO}1054 and 1013 (S-DMSO), $\nu_{C=C}$ (pyz) 1629, $\nu_{C=N}$ (pyz) 1400; UV-vis (H_2O): 386 nm ($\varepsilon = 1393\ L{\cdot}mol^{-1}{\cdot}m^{-1}$); 386 nm ($\varepsilon = 13495\ L{\cdot}mol^{-1}{\cdot}m^{-1}$).

3. Result and Discussion

The IR spectra of **2** shows the disappearance of N–H vibrations, suggesting coordination of pyrazole. The uncoordinated pyrazole C=C and C=N stretching modes observed at 1640 and 1558 cm^{-1} are altered significantly at lower frequencies. This is consistent with longer C=C and C=N bonds in these complexes compared with the same distances in the uncoordinated ligand [20]. The stretching band of *mer*-$RuCl_3(DMSO)_3$ is shifted to a lower frequency compared to **2**. The stretching bands found at 1062 cm^{-1} are assigned to the coordinated S-DMSO.

The formulation of compound **2** (Figure 1), *mer*-$[RuCl_3(DMSO)\ (pyrazole)_2]$, was further established by X-ray analysis, indicating that it crystallizes in the monoclinic space group $P2_1/n$ with distorted octahedral geometry (Figure 1). The cell parameters and crystal data for compound *mer*-$[RuCl_3(DMSO)\ (pyrazole)_2]$ are listed in Tables 1 and 3. The Ru^{3+} is coordinated by six donors: S of one DMSO, two pyrazole nitrogens, and three meridional chloro ligands. One pyrazole is *trans* to the S-DMSO ligands and the other is *trans* to one of the chloro ligands, and the both pyrazole ligands are *cis* to each other.

The X-ray analysis revealed two independent molecules in the asymmetric unit cell (Figure 1). The two independent molecules differ in the relative conformations of the two pyrazole ligands. In one molecule, the N3-Ru1-N1-N2 torsion angle -122.2(2)°, while in the other, the corresponding torsion angle N7-Ru2-N5-N6 is +88.3(2)°. Thus, this pyrazole differs in conformation by about 146° between the two independent molecules, likely because of the difference in hydrogen bonding between the two molecules, vide infra. The average Ru-S bond length of **2**, 2.2845 Å, is markedly shorter than the average value of 2.34(1) Å found, for the Ru(III)-S compounds *trans* to DMSO-S in the precursor [21, 22]. The average Ru-Cl bond length of **2**, 2.3500 Å, is equivalent to the mean value of 2.350(7) Å witnessed in related Ru(III) complexes [23–25]. The N1-Ru1-S1, 178.57(11)°, and Cl2-Ru1-Cl3, 176.78(9)° bond angles are slightly smaller than the known values of octahedral Ru(III) complexes [23–25].

In both independent molecules, one pyrazole forms an intramolecular hydrogen bond to DMSO oxygen, while the other pyrazole forms a bifurcated intramolecular/intermolecular hydrogen bond, where the intramolecular component is to Cl. For one of the independent molecules, the intermolecular component is to DMSO oxygen, while for the other, it is to Cl. Thus, one independent molecule (containing Ru2) forms hydrogen bonded chains, while the other (containing Ru1) forms centrosymmetric hydrogen bonded dimers (Figures 2(a), 2(b), and Table 3).

4. Chemical Behavior in Aqueous Solution

The electronic spectra of compound **2** (aqueous solution) show an intense absorption between 300 and 400 nm, accompanying with a less intense transition around 450 nm. This spectral pattern is allocated to a charge transfer transition from the Cl^- to Ru^{3+} [26, 27]. This is distinctive for a $RuCl_4^-$ unit. We followed the time-course profile of electronic spectral behavior in an aqueous solution of compound **2**. A solution of complex (0.0005 M) in deionized water was prepared and analyzed in UV-visible for 8 hours at 37°C and 50°C (Figures 3(a) and 3(b)). The changes observed in the UV/vis-spectra suggest the formation of a hydrolysis product of **2** in a water solution (Scheme 1). The original spectrum of compound **2** with a maximum at 361 nm changes to give a spectrum with a maximum at 330 nm after 6 hours as can be seen in Figures 2 and 3. The isosbestic point at 330 nm indicates a transformation into a hydrolysis product (Scheme 1). Qualitatively a similar behavior is also observed for NAMI-A under similar conditions [28]. This behavior could be explained by stepwise chloride hydrolysis. The activation mechanism of Ru complexes has been described recently [29].

5. DFT Calculation

Ru(III) Hydrolysis. It is generally accepted that the hydrolysis or water exchange of the metal complex is the key step attributed to the cytotoxicity of the drug. Therefore, we have

Table 1: Crystal data and structure refinement for mer-[$RuCl_3$(DMSO) (pyrazole)$_2$] **2**.

Formula	$C_8H_{14}Cl_3N_4ORuS$
Molar Mass	421.71
Crystal system	Monoclinic
T (K)	90
a (Å)	8.0596
b (Å)	12.6816
c (Å)	29.278
β (°)	90.617
h, k, l limits	$-11 \longrightarrow 11$; $-18 \longrightarrow 17$; $-42 \longrightarrow 42$
Z	8
Θ range (°)	2.5–31.0
μ (mm^{-1})	1.72
R [$F^2 > 2\sigma(F^2)$]	0.034
R	0.038
wR(F^2)	0.074

Table 2: Bond length and bond angle of compounds 2.

Bond length (Å)			
Ru1-N3	2.062	**Ru2-N7**	2.067
Ru1-N1	2.092	Ru2-N5	2.091
Ru1-S1	2.2940	Ru2-S2	2.2745
Ru1-Cl1	2.3517	Ru2-Cl4	2.3290
Ru1-Cl2	2.3635	Ru2-Cl5	2.3477
Ru1-Cl3	2.3464	Ru2-Cl7	2.3622
Bond angle (°)			
N3-Ru1-N1	88.05	N7-Ru2-N5	87.82
N3-Ru1-S1	95.21	N7-Ru2-S2	97.12
N1-Ru1-S1	174.85	N5-Ru2-S2	174.48
N3-Ru1-Cl3	88.62	N7-Ru2-Cl5	174.32
N1-Ru1-Cl3	88.14	N5-Ru2-Cl5	86.80
S1-Ru1-Cl3	87.96	S2-Ru2-Cl5	88.34
N3-Ru1-Cl1	88.88	N7-Ru2-Cl4	84.67
N1-Ru1-Cl1	89.91	N5-Ru2-Cl4	90.93
S1-Ru1-Cl1	94.12	S2-Ru2-Cl4	91.98
Cl3-Ru1-Cl1	176.88	Cl5-Ru2-Cl4	93.58
N3-Ru1-Cl2	176.24	N7-Ru2-Cl6	85.52
N1-Ru1-Cl2	88.85	N5-Ru2-Cl6	90.57
S1-Ru1-Cl2	88.03	S2-Ru2-Cl6	87.37
Cl3-Ru1-Cl2	93.40	Cl5-Ru2-Cl6	96.36
Cl1-Ru1-Cl2	88.99	Cl4-Ru2-Cl6	170.01

considered several hydrolysis pathways for both **2** and **1** [29]. Our focus in the current study is to compare the hydrolysis pathways for both **2** and **1(III)** (Figure 4(a)).

In line with experimental studies on NAMI and NAMI-A, hydrolysis of a nitrogen-based ligand requires large activation energies, and the reaction is hugely endothermic. Therefore, it is very unlikely that the Pyz-water exchange will take place under neutral conditions. Thus, we have focused on DMSO and Cl^- hydrolysis. We have found two pathways for the first hydrolysis of **1(III)** (Figure 4(a)). In path 1 (Scheme 1), the incoming water displaces the DMSO ligand with an activation energy of 31.6 kcal/mol, which is larger than the DMSO dissociation in NAMI (23.7 kcal/mol). This may be partly caused by the weakening of the O–HN hydrogen bond in the transition state as the hydrogen bond length increases from 1.728 Å in **1(III)** to 2.359 Å in **1(III)a**. The water exchange reaction is slightly exothermic (−4.0 kcal/mol). On the other hand, in the second pathway, a Cl^- ligand is replaced by water. The activation energy (35.5 kcal/mol) is comparable to that of DMSO dissociation and to NAMI; however, the reaction is endothermic (6.7 kcal/mol) and therefore less favorable. Thus, both kinetic and thermodynamic parameters suggest that the first hydrolysis step involves DMSO-water exchange. The second hydrolysis step proceeds faster as the activation free energy of a Cl^- exchange with water decreases by ~5 kcal/mol (**1c**, Figure 4(b)). The lowering of activation energy is mainly due to the strong hydrogen bonding between the leaving Cl^- ligand and the two water molecules, one of which is incoming and the other is already present (**1(III)c**). Again, the reaction is slightly exothermic (−2.36 kcal/mol). Thus, the overall reaction, the exchange of DMSO and Cl^- ligand with two water molecules, is exothermic (−6.34 kcal/mol).

Ru(II) Hydrolysis. The biological diversity of **1(III)** may also be due to its contrasting redox properties. The reduction potentials for **1(III)** is 0.04 V. Since the E_m for **1(III)** is positive, it might be easily reduced under biological conditions. In case of NAMI-A, there is some evidence that the reduced form plays an important role in its cytotoxicity. Therefore, it is important to consider the hydrolysis behavior of the reduced species as well. We have calculated the reaction pathways of the reduced forms of **1** (Figures 4(a) and 4b).

Once again, we have considered two reaction pathways (DMSO and Cl^-) for **1(II)**. The first hydrolysis step, the activation free energy of Cl^- and DMSO is very similar (27.40 and 28.2 kcal/mol, respectively), which are smaller (by ~8.0 kcal/mol) than the corresponding numbers for Ru(III) and comparable to the NAMI-A activation energies (28.8 kcal/mol). These numbers are in line with the experimental observations that Ru(II) is kinetically more labile than Ru(III). The reaction-free energies for Cl^- and DMSO are −3.00 and 0.66 kcal/mol, respectively. It is likely that the first dissociation might be Cl^- because Cl^- hydrolysis is more exothermic. The second hydrolysis pathway involves Cl^- hydrolysis with the activation-free energy of (21.1 kcal/mol).

Over all, the thermodynamic and kinetic analysis of the hydrolysis reactions for Ru(III) and Ru(II) complex of **1** show an interesting pattern. In both Ru(III) and the reduced form Ru(II), compound **1** undergoes hydrolysis under physiological conditions. This study demonstrates that redox properties play a significant role in the hydrolysis mechanism and consequently in their biological activity.

6. Electrochemical Study

Cyclic voltammetry was carried out with a three-electrode system comprised of a Pt counter electrode, a Pt disk working electrode, and a saturated calomel electrode (SCE) connected to the main cell compartment by a KCl salt bridge. Potential control was done with a BAS CV-50 W voltammetric analyzer used in the cyclic voltammetry mode.

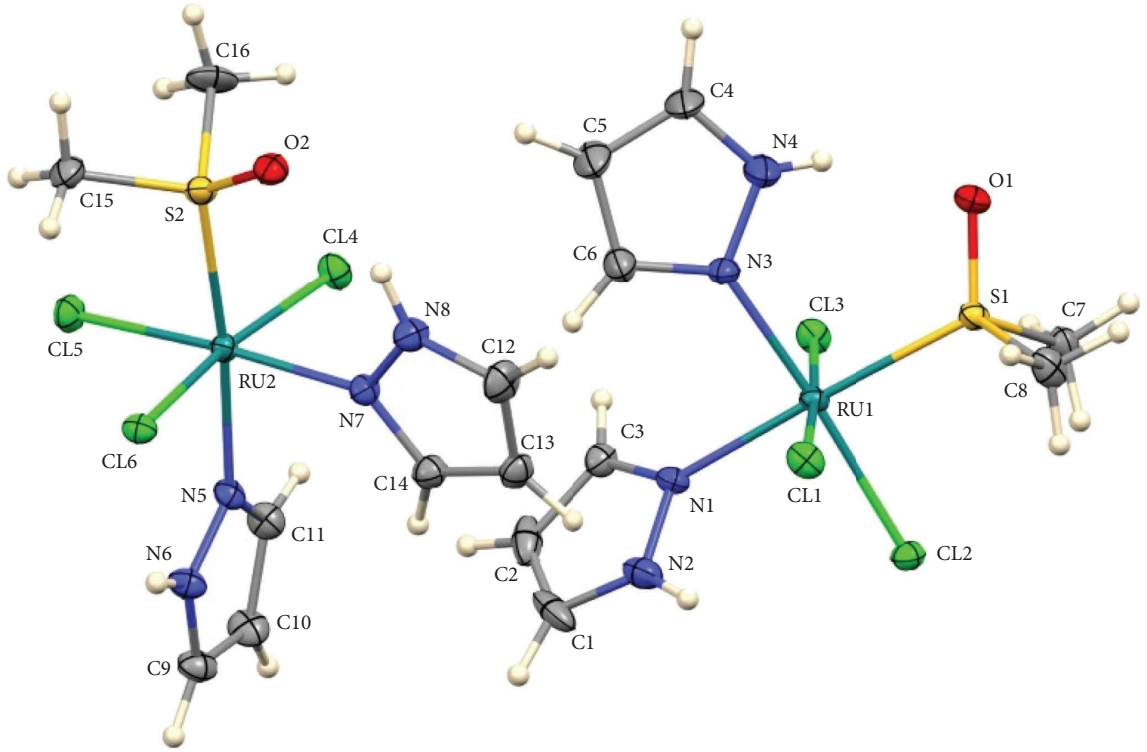

Figure 1: Asymmetric unit of compound 2, with 50% ellipsoids.

Table 3: Hydrogen-bond geometry (Å) for (Compound 2).

D—H—*A*	*D*—H	H—*A*	*D*—*A*	*D*—H—*A*
N2—H2*N*—Cl1	0.96 (3)	2.68 (3)	3.252 (3)	119 (2)
N2—H2*N*—Cl2^{i}	0.96 (3)	2.63 (3)	3.350 (2)	132 (2)
N4—H4*N*—O1	0.77 (3)	1.97 (3)	2.691 (3)	155 (3)
N6—H6*N*—Cl6	0.93 (3)	2.46 (3)	3.098 (2)	126 (2)
N6—H6*N*—O2^{ii}	0.93 (3)	2.12 (3)	2.887 (3)	139 (2)
N8—H8*N*—O2	0.92 (3)	1.91 (3)	2.754 (3)	152 (3)

Symmetry codes: (i) $-x+1, -y, -z+1$; (ii) $-x+3/2, y-1/2, -z+1/2$.

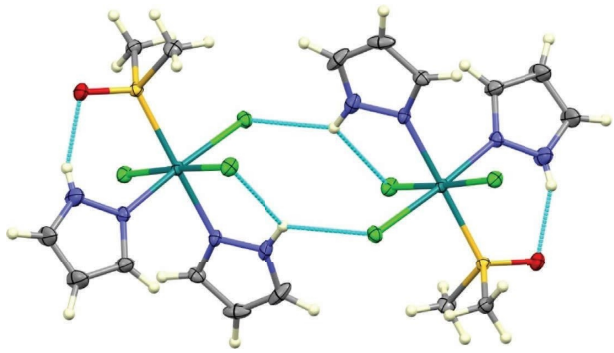

(a)

Figure 2: Continued.

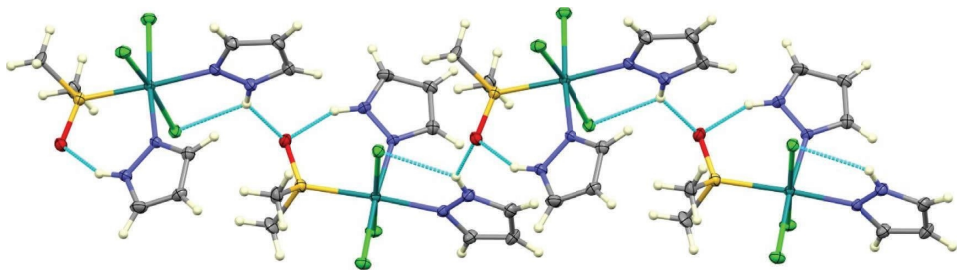

(b)

Figure 2: (a) Hydrogen bonded dimer formed by the Ru1 molecule. (b) Hydrogen bonded chain formed by the Ru2 molecule.

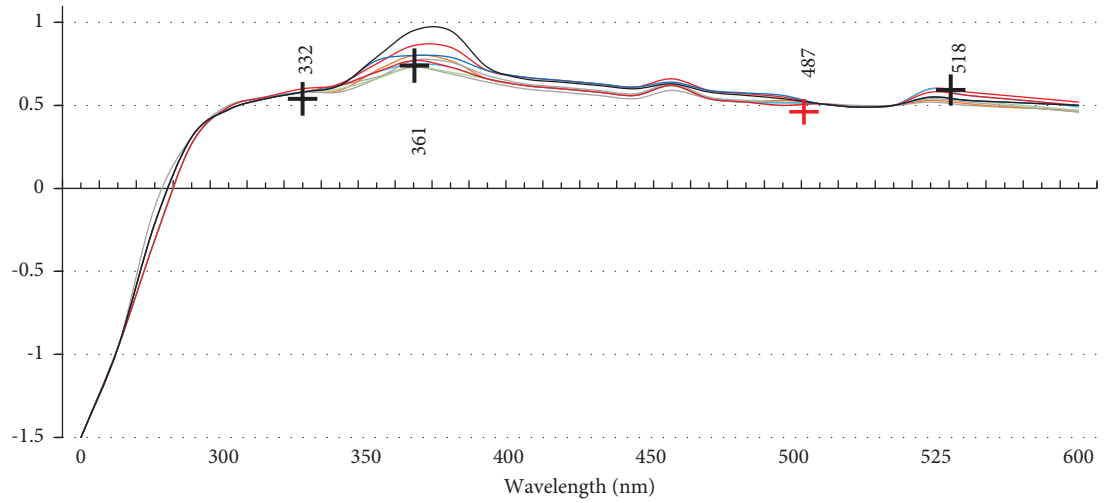

(a)

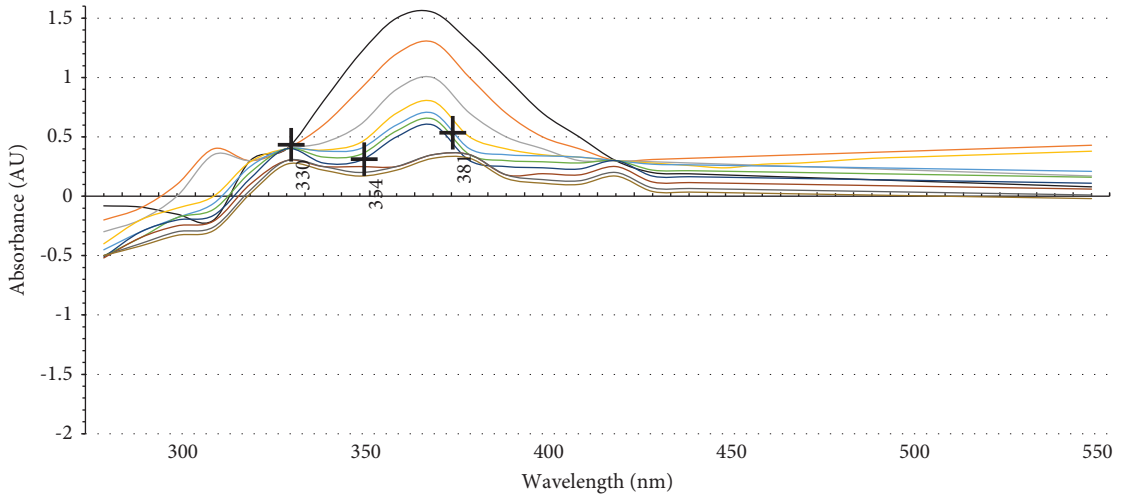

(b)

Figure 3: (a) UV-Vis spectra recorded at 37°C. (b) UV-vis spectra recorded at 50°C.

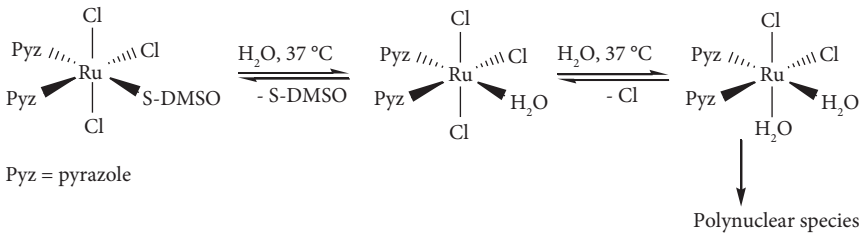

Scheme 1: DFT calculated stepwise hydrolysis of compound 2.

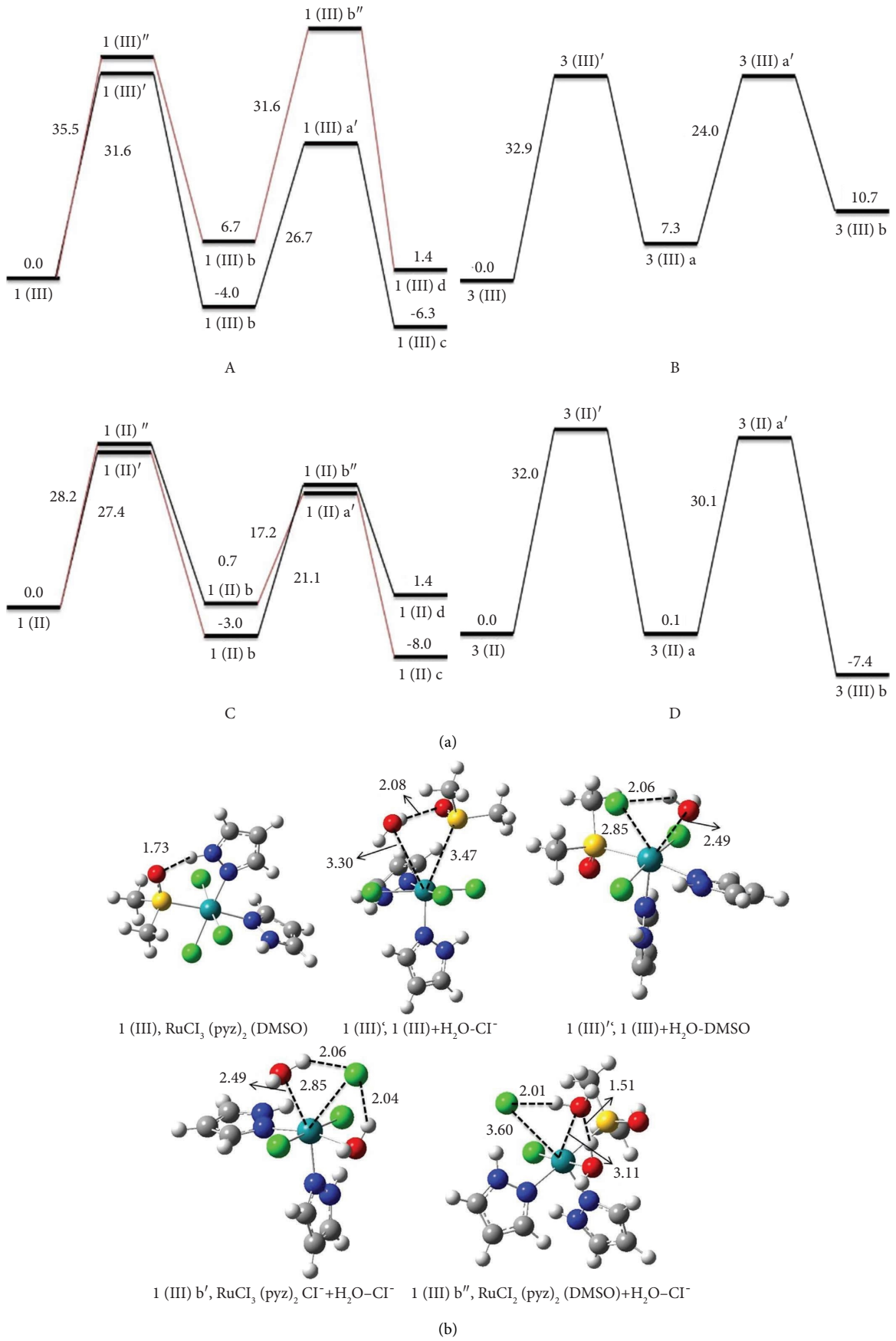

Figure 4: (a) Optimized structures of **1(III)** and **3(III)** and the structures of transition states along with selected bond lengths (Å). Model of optimized structures. (b) Hydrolysis free energy profiles of (a) **1(III)**, $RuCl_3(pyz)_2(DMSO)$ with water. Black lines indicate the hydrolysis of DMSO followed Cl^-, and red lines indicate the hydrolysis of Cl^- and Cl^-, respectively (B)

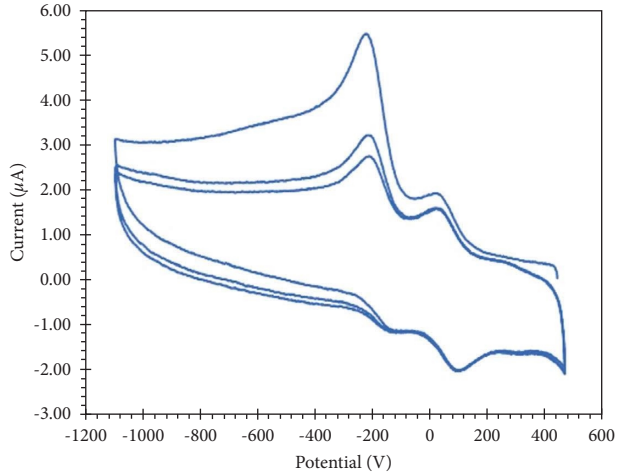

Figure 5: Cyclic voltammetry.

The supporting electrolyte was 0.100 M tetrabutylammonium hexafluorophosphate in DMSO solutions and KCl in aqueous solutions. Argon was bubbled through the solution for at least 30 min prior to the final cell setup. Cyclic voltammetry was done in quiescent solutions. Argon was then bubbled through the same solution, and the setup was reused to obtain cyclic voltammograms at higher sweep rates. The initial direction of voltammetry was negative, or cathodic, except for solutions containing ferrocene and anything otherwise was noted.

Figure 5 shows cyclic voltammetry results in DMSO for **1**. Two redox couples are evident. Averaging over the sweep rates covered, the values of the formal potentials calculated from the voltammograms were found to be −0.174 V and 0.058 V. Semiderivative analyses gave values of −0.170 V and 0.061 V [30, 31]. These couples are consistent with one electron oxidations and reductions between the +3, +2, and +1 oxidation states of Ru.

At 100 mV/s only, the range was extended anodic of the open circuit potential at which all the cyclic voltammetry experiments were begun. Two other redox couples were observed: a small pair of redox peaks centered at 0.294 V and a large pair of peaks centered at 0.539 V.

7. Conclusion

A new class of water-soluble ruthenium-based anticancer drugs of pyrazole ligand has been synthesized. The complex was completely characterized by various spectroscopic and X-ray studies. Our experimental observations of the hydrolysis of compound **2** established that it hydrolyzed stepwise. This is in line with NAMI-A hydrolysis. DFT calculations have also established that in the neutral compound **2,** first DMSO is exchanged, followed by chloride ion.

Data Availability

Crystal structure data in CIF format (CCDC 806296) can be obtained from the Cambridge Crystallographic Data Centre (CCDC) at https://www.ccdc.cam.ac.uk.

Conflicts of Interest

The authors declare that there are no conflicts of interest.

Authors' Contributions

Dr. Radhey S. Srivastava designed and conceived the research. Mylene Panques and Arushi Shyam performed synthesis. Dr. R. S. Perkins and Dr. Frank. R. Fronczek contributed to DFT and cyclovoltameter and X-ray diffraction studies of compound 2.

Acknowledgments

The authors are grateful for financial support from the University of Louisiana-Lafayette and Louisiana Board of Regents (LEQSF (2009–12)-RD-B-08).

References

[1] T. Boulikas and M. Vougiouka, "Cisplatin and platinum drugs at the molecular level (review)," *Oncology Reports*, vol. 10, p. 1663, 2003.

[2] E. Wong and C. M. Giandomenico, "Current status of platinum-based antitumor drugs," *Chemistry Review*, vol. 99, no. 9, pp. 2451–2466, 1999.

[3] M. Galanski, V. B. Arion, M. A. Jakupec, and B. K. Keppler, "Recent developments in the field of tumor-inhibiting metal complexes," *Current Pharmaceutical Design*, vol. 9, no. 25, pp. 2078–2089, 2003.

[4] Z. Ai, Y. Lu, S. Qiu, and Z. Fan, "Overcoming cisplatin resistance of ovarian cancer cells by targeting HIF-1-regulated cancer metabolism," *Cancer Letters*, vol. 373, no. 1, pp. 36–44, 2016.

[5] D. W. Shen, L. M. Pouliot, M. D. Hall, and M. M. Gottesman, "Cisplatin resistance: a cellular self-defense mechanism resulting from multiple epigenetic and genetic changes," *Pharmacological Reviews*, vol. 64, no. 3, pp. 706–721, 2012.

[6] R. J. Parker, A. Eastman, F. Bostick-Bruton, and E. Reed, "Acquired cisplatin resistance in human ovarian cancer cells is associated with enhanced repair of cisplatin-DNA lesions and

reduced drug accumulation," *Journal of Clinical Investigation*, vol. 87, no. 3, pp. 772–777, 1991.

[7] S. Page, "Ruthenium compounds as anticancer agents," *Education in Chemistry*, vol. 10, p. 26, 2012.

[8] A. Sigel and H. Sigel, "Metal ions in biological systems," *Metal Complexes in Tumor Diagnosis and as Anticancer Agents*, Marcel Dekker, New York, NY, USA, 2004.

[9] L. Ronconi and P. J. Sadler, "Using coordination chemistry to design new medicines," *Coordination Chemistry Reviews*, vol. 251, no. 13-14, pp. 1633–1648, 2007.

[10] P. J. Dyson and G. Sava, "Metal-based antitumour drugs in the post genomic era," *Dalton Transactions*, vol. 1929, no. 16, pp. 1929–1933, 2006.

[11] C. X. Zhang and S. J. Lippard, "New metal complexes as potential therapeutics," *Current Opinion in Chemical Biology*, vol. 7, no. 4, pp. 481–489, 2003.

[12] S. Y. Lee, C. Y. Kim, and T. G. Nam, "Ruthenium complexes as anticancer agents: a brief history and perspectives," *Drug Design, Development and Therapy*, vol. 14, p. 5375, 2020.

[13] G. Sava and A. Bergamo, "Ruthenium-based compounds and tumour growth control (review)," *International Journal of Oncology*, vol. 17, no. 2, pp. 353–365, 2000.

[14] Y. Q. Gu, W. Y. Shen, Q. Y. Yang, Z. F. Chen, and H. Liang, "Ru(iii) complexes with pyrazolopyrimidines as anticancer agents: bioactivities and the underlying mechanisms," *Dalton Transition*, vol. 51, p. 1333, 2022.

[15] J. Coverdale, T. Laroiya-McCarron, I. Romero-Canelón, and I. Romero-Canelón, "Designing ruthenium anticancer drugs: what have we learnt from the key drug candidates?" *Inorganics*, vol. 7, no. 3, p. 31, 2019.

[16] M. J. Clarke, "Ruthenium metallopharmaceuticals," *Coordination Chemistry Reviews*, vol. 236, no. 1-2, pp. 209–233, 2003.

[17] R. Trondl, P. Heffeter, C. R. Kowol, M. A. Jakupec, W. Berger, and B. K. Keppler, "NKP-1339, the first ruthenium-based anticancer drug on the edge to clinical application," *Chemical Science*, vol. 5, no. 8, pp. 2925–2932, 2014.

[18] E. Alessio and L. Messori, "NAMI-A and KP1019/1339, two iconic ruthenium anticancer drug candidates face-to-face: a case story in medicinal inorganic chemistry," *Molecules*, vol. 24, no. 10, p. 1995, 2019.

[19] E. Alessio, G. Balducci, M. Calligaris, G. Costa, W. M. Attia, and G. Mestroni, "Synthesis, molecular structure, and chemical behavior of hydrogen trans-bis (dimethyl sulfoxide) tetrachlororuthenate (III) and mer-trichlorotris (dimethyl sulfoxide) ruthenium (III): the first fully characterized chloride-dimethyl sulfoxide-ruthenium (III) complexes," *Inorganic Chemistry*, vol. 30, no. 4, pp. 609–618, 1991.

[20] H. W. W. Ehrlich, "The crystal and molecular structure of pyrazole," *Acta Crystallographica*, vol. 13, no. 11, pp. 946–952, 1960.

[21] J. S. Jaswal, S. J. Rettig, and B. R. James, "Ruthenium (III) complexes containing dimethylsulfoxide or dimethylsulfide ligands, and a new route to trans-dichlorotetrakis (dimethylsulfoxide) ruthenium (II)," *Canadian Journal of Chemistry*, vol. 68, no. 10, pp. 1808–1817, 1990.

[22] R. S. Srivastava and F. R. Fronczek, "Unexpected formation and structure elucidation of mer-[RuCl3(TMSO)(bpy)] derived from [H(TMSO)] [trans-RuCl4(TMSO)2] under mild condition," *Inorganica Chimica Acta*, vol. 358, no. 3, pp. 854–857, 2005.

[23] E. Alessio, G. Balducci, A. Lutman, G. Mestroni, M. Calligaris, and W. Attia, "Synthesis and characterization of two new classes of ruthenium (III)-sulfoxide complexes with nitrogen donor ligands (L): Na[trans-$RuCl_4(R_2SO)(L)$] and mer, cis-$RuCl_3(R_2SO)(R_2SO)(L)$. The crystal structure of Na[trans-$RuCl_4$(DMSO)(NH_3)] 2DMSO, Na[trans-$RuCl_4$(DMSO)(Im)] H_2O, Me_2CO (Im = imidazole) and mer, cis-$RuCl_3$(DMSO)(DMSO)(NH_3)," *Inorganica Chimica Acta*, vol. 203, no. 2, pp. 205–217, 1993.

[24] M. Calligaris, N. Bresciani-Pahor, and R. S. Srivastava, "Structure of acridinium trans-tetrachlorobis (dimethyl sulfoxide) ruthenate (III)," *Acta Crystallographica Section C Crystal Structure Communications*, vol. 49, no. 3, pp. 448–451, 1993.

[25] M. Calligaris, "Structure and bonding in metal sulfoxide complexes: an update," *Coordination Chemistry Reviews*, vol. 248, no. 3-4, pp. 351–375, 2004.

[26] C. M. Duff and G. A. Heath, "From [RuX6] to [Ru(RCN)6]: synthesis of mixed halide–nitrile complexes of ruthenium, and their spectroelectrochemical characterization in multiple oxidation states," *Dalton Transactions*, vol. 9, p. 2401, 1991.

[27] G. Mestroni, E. Alessio, G. Sava, S. Pacor, M. Coluccia, and A. Boccarelli, "Water soluble ruthenium(III)dimethyl sulfoxide complexes: chemical behavior and pharmaceutical properties," *Met. Based Drugs*, vol. 1, p. 4, 1993.

[28] M. Pal, U. Nandi, and D. Mukherjee, "Detailed account on activation mechanisms of ruthenium coordination complexes and their role as antineoplastic agents," *European Journal of Medicinal Chemistry*, vol. 150, pp. 419–445, 2018.

[29] A. Kung, T. Pieper, R. Wissiack, E. Rosenberg, and B. K. Keppler, "Hydrolysis of the tumor-inhibiting ruthenium(III) complexes HIm trans-[$RuCl_4$(im)2] and Hind trans-[$RuCl_4$(ind)2] investigated by means of HPCE and HPLC-MS," *Journal of Biological Inorganic Chemistry*, vol. 6, no. 3, pp. 292–299, 2001.

[30] P. Dalrymple-Alford, M. Goto, and K. B. Oldham, "Shapes of derivative neopolarograms," *Journal of Electroanalytical Chemistry and Interfacial Electrochemistry*, vol. 85, pp. 1–15, 1977.

[31] P. Dalrymple-Alford, M. Goto, and K. B. Oldham, "Peak shapes in semidifferential electroanalysis," *Analytical Chemistry*, vol. 49, no. 9, pp. 1390–1394, 1977.